



HAL
open science

A new technique to generate independent periodic attractors in the state space of nonlinear dynamic systems

Cristina Morel, Radu Vlad, Eric Chauveau

► **To cite this version:**

Cristina Morel, Radu Vlad, Eric Chauveau. A new technique to generate independent periodic attractors in the state space of nonlinear dynamic systems. *Nonlinear Dynamics*, 2010, 59 (1-2), pp.45-60. 10.1007/s11071-009-9519-7 . hal-01202707

HAL Id: hal-01202707

<https://hal.science/hal-01202707>

Submitted on 23 Feb 2018

HAL is a multi-disciplinary open access archive for the deposit and dissemination of scientific research documents, whether they are published or not. The documents may come from teaching and research institutions in France or abroad, or from public or private research centers.

L'archive ouverte pluridisciplinaire **HAL**, est destinée au dépôt et à la diffusion de documents scientifiques de niveau recherche, publiés ou non, émanant des établissements d'enseignement et de recherche français ou étrangers, des laboratoires publics ou privés.

A new technique to generate independent periodic attractors in the state space of nonlinear dynamic systems

Cristina Morel, Radu Vlad, Eric Chauveau

C. Morel, E. Chauveau
École Supérieure d'Électronique de l'Ouest—ESEO,
4, rue Merlet de la Boulaye, 49009 Angers, France
e-mail: cristina.morel@eseo.fr

E. Chauveau
e-mail: eric.chauveau@eseo.fr

R. Vlad
Technical University of Cluj-Napoca, 103-105,
Bd. Muncii, 400641 Cluj-Napoca, Romania
e-mail: radu.constantin.vlad@mis.utcluj.ro

Abstract This paper proposes a method to generate several independent periodic attractors, in continuous-time nonchaotic systems (with an equilibrium point or a limit cycle), based on a switching piecewise-constant controller. We demonstrate here that the state space equidistant repartition of these attractors is on a precise zone of a precise curve that depends on the parameters of the system. We determine the state space domains where the attractors are generated from different initial conditions. A mathematical formula giving their maximal number in function of the controller piecewise-constant values is then deduced. Throughout this study, the proposed methodology is illustrated with several examples.

Keywords Anticontrol of chaos · Independent periodic attractors · Initial conditions · Switching piecewise-constant controller

1 Introduction

The study of chaotic dynamics has evolved from the traditional trend of understanding and analyzing chaos to the new attempt of controlling and utilizing it. Recently, there has been increasing interest in exploiting chaotic dynamics in engineering applications, such as telecommunications [1–4], information processing [5], electrical engineering [6], whereas much attention has focused on effectively generating chaos.

It is well known that chaos can be generated via different approaches, such as linear feedback techniques or switching methods, to obtain various chaotic attractors [7–9] from the new chaotic system [8, 10] or circuits [11, 12]. Another technique to create chaos is to use a time-delay feedback perturbation on a system parameter or to employ an exogenous time-delay state-feedback input. This chaotic reference method designs a simple nonlinear feedback controller with an arbitrarily small amplitude leading to a chaotic dynamics in the controlled system [13, 14].

The effect of time delay on the differential system can be observed in [15–17], with coexisting trivial attractors (fixed points or limit cycles) and strange attractors. A similar phenomenon generating various limit cycles is presented in [18] and [19]. In [18], two sets of initial conditions produce two different limit cycles and a new limit cycle for each new initial condition selected is observed in [19].

After the study of the harmonics of chaotic [20, 21] or nonchaotic [22] systems, we generated attractors using a switching piecewise-binary controller in a precise but uncontrollable area of the state space [23]. This time, we propose a switching piecewise-constant controller in continuous-time systems to generate several independent chaotic attractors in a controllable state space area. The attractors are reached from different initial conditions and are generated on a precise zone of a precise curve in the state space. The generation of the attractors in the state space domain respects the following analysis steps of the nonlinear system:

- Parameterization of the nonlinear system and calculus of its equilibria; their graphical representation in function of the parameter gives a precise curve in the state space;
- Determination of the parameter variation domain so that the equilibria of the nonlinear parameterized system are stable;
- Determination of the state space domains where the attractors are generated;
- Replacement of the static variation of the parameter with a fast dynamics variation (a switching piecewise-constant controller) to generate several independent chaotic attractors around the stable equilibria; this controller represents a nonlinear feedback, as a sine function of the system state; the sine anticontrol feedback frequency imposes an attractor periodicity in the state space;
- Determination of the attractors maximal number in function of the piecewise-constant controller values and the sine anticontrol feedback frequency.

Throughout this study, the proposed methodology is illustrated with three examples: the Lorenz, Van der Pol and Jerk systems.

2 Equilibria of a nonlinear system

Consider an N -dimensional nonlinear system of the following form:

$$\begin{cases} \dot{x}_1 = f_1(\mathbf{x}(t), p), \\ \dot{x}_2 = f_2(\mathbf{x}(t)), \\ \vdots \\ \dot{x}_N = f_N(\mathbf{x}(t)), \end{cases} \quad (1)$$

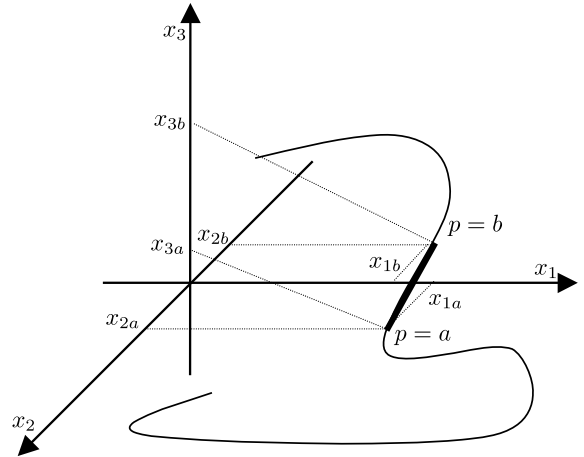


Fig. 1 Example of the system (1) equilibria on three-dimensional state space

where $\mathbf{x}(t) = [x_1(t), x_2(t), \dots, x_N(t)]$ is the state vector, p a real parameter and f_i , for $i = \overline{1, N}$, are nonlinear functions. The equilibria of the system (1) are found by solving the equations $\dot{x}_i = 0$, for $i = \overline{1, N}$, and represent the roots of the following equations:

$$\begin{cases} f_1(\mathbf{x}(t), p) = 0, \\ f_2(\mathbf{x}(t)) = 0, \\ \vdots \\ f_N(\mathbf{x}(t)) = 0. \end{cases} \quad (2)$$

For the parameterized system (1), the graphical representation of these equilibria depending on the parameter p gives a precise curve in the state space. An example of three-dimensional state space (x_1, x_2 and x_3) of the equilibria is presented on Fig. 1 by the fine curve.

Considering a Jacobian matrix for the equilibria and calculating its characteristic equation, we can investigate the stability of each equilibrium based on the Routh–Hurwitz conditions of the system characteristic equation. We determine the parameter variation domain such that the equilibria of the nonlinear parameterized system are stable. Let us take into account a variation of the parameter p for which the equilibria are stable as follows:

$$a \leq p \leq b. \quad (3)$$

For p between a and b , the stable equilibria take values in the N -dimensional domain of the state space:

$$\left\{ \begin{array}{l} \text{on } x_1 \text{ axis: } [x_{1a}; x_{1b}], \\ \text{on } x_2 \text{ axis: } [x_{2a}; x_{2b}], \\ \vdots \\ \text{on } x_N \text{ axis: } [x_{Na}; x_{Nb}]. \end{array} \right. \quad (4)$$

Figure 1 presents an example of the stable equilibria (the bold curve) on the three-dimensional state space (x_1 , x_2 and x_3). In this paper, we are interested in generating several independent chaotic attractors in the N -dimensional domain (4), on the bold curve of Fig. 1, by switching the control parameter p among the values a and b .

3 Generating independent chaotic attractors in a nonlinear system

In the previous section, we have considered a static variation of the parameter p . Recently, [15–17] have considered a periodic nonlinearity of p as $\mu \sin(x(t - \tau))[1 + \varepsilon \sin(x^2(t - \tau))]$. The global behavior of the delay model shows the coexistence of trivial attractors (fixed point or limit cycle) and chaotic attractors (with stable and unstable equilibria) generated in the precise state space. With another nonlinear function p as $\varepsilon \sin(\sigma x(t - \tau))$, [14] obtains only two separated chaotic attractors near two stable fixed points for large values of σ .

In this section, we propose a controller to generate several independent chaotic attractors in the state space. A control engineering application is to make a nonlinear system converge to some attractors of interest, starting from different initial conditions, in order to reach different regimes of operation.

In order to generate independent chaotic attractors for the system (1), we specify a piecewise-constant characteristic of the feedback controller p , defined analytically as follows:

$$p = \begin{cases} b, & g(t) < u(\mathbf{x}(t)) \\ a, & g(t) \geq u(\mathbf{x}(t)), \end{cases} \quad (5)$$

where $g(t)$ is a periodic function and $u(t)$ the anti-control of chaos state feedback. We propose to use the anti-control of chaos state feedback together with a

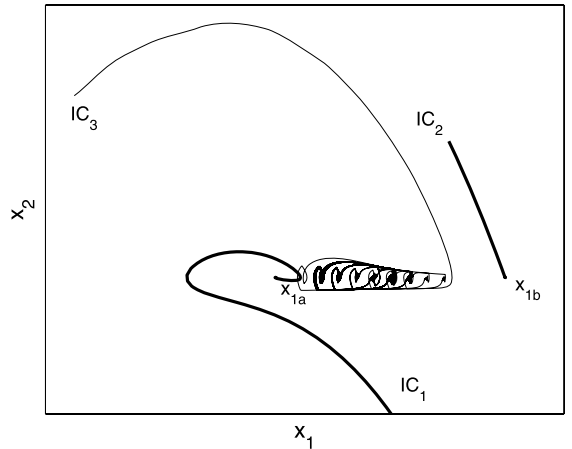


Fig. 2 Two stable equilibria or a chaotic attractor

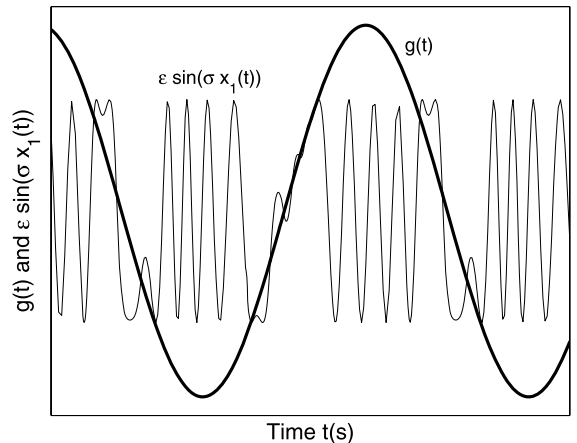


Fig. 3 Slow dynamics of $g(t)$: example of sinus function $g(t)$ and the anticontrol of chaos state feedback $u(\mathbf{x}(t))$

piecewise-constant controller, hereafter denoted anti-control switching piecewise-constant controller of (5). We give now details about the choice of the waveform, the amplitude and frequency of $g(t)$ and $u(\mathbf{x}(t))$. The application of the classical method [13, 14, 20] of chaos anticontrol to obtain a chaotic dynamic in the controlled system (1) uses a nonlinear state feedback. We are interested by a sine function

$$u(\mathbf{x}(t)) = \varepsilon \sin(\sigma x_1(t)), \quad (6)$$

as in [14, 23]. If $g(t) \geq u(\mathbf{x}(t))$, p is always equal to a . Starting from any initial condition IC_1 , the state variable x_1 converges to x_{1a} as shown in Fig. 2. For the case $g(t) < u(\mathbf{x}(t))$ (so p is always equal to b), the

same figure shows that the state variable x_1 converges to x_{1b} starting from IC_2 .

On the other hand, supposing that $g(t)$ has a large amplitude and a slow dynamics in comparison with $u(\mathbf{x}(t))$, Fig. 3 shows an example of a sine function $g(t)$ and the anticontrol of chaos state feedback $u(\mathbf{x}(t))$, which determines a slow switching of the controller of (5) between the levels a and b . Starting from the initial condition IC_3 , the state variable x_1 has a large variation attracted into an attractor as in Fig. 2.

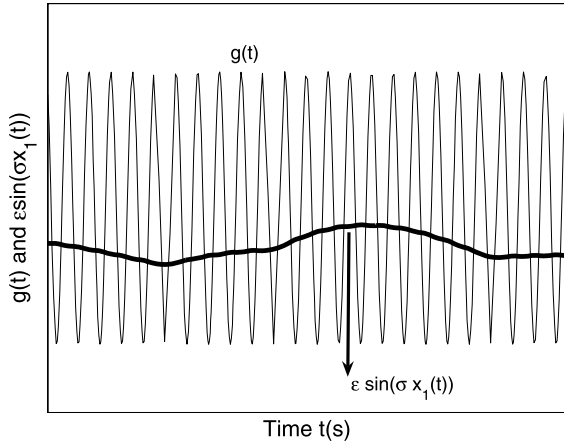
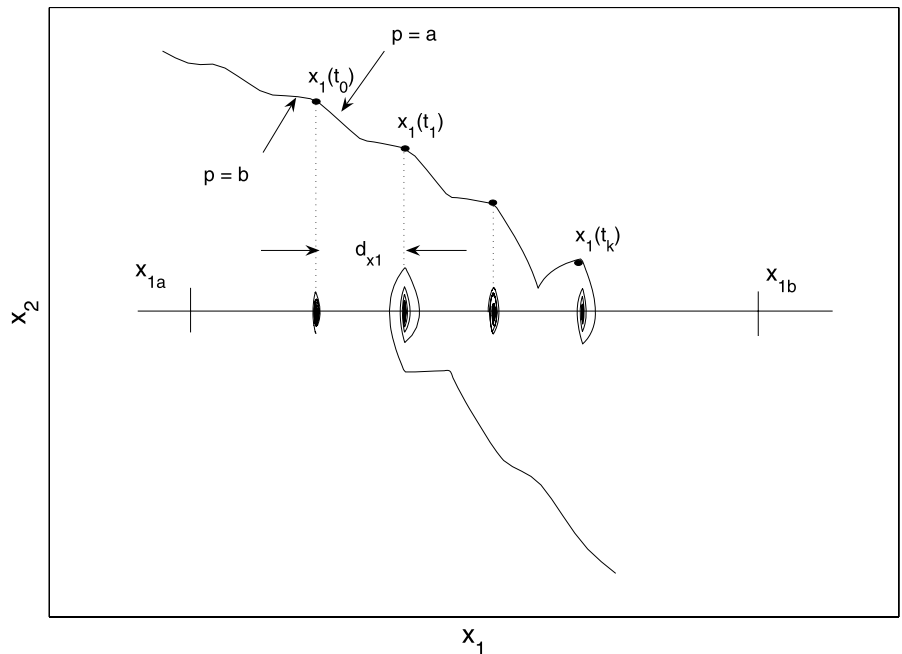


Fig. 4 Fast dynamics of $g(t)$: example of sinus function $g(t)$ and the anticontrol of chaos state feedback $u(\mathbf{x}(t))$

Fig. 5 Example of independent chaotic attractors



In this paper, we are interested in a fast dynamics of the periodic function

$$g(t) = \sin(\gamma t), \quad (7)$$

as in Fig. 4. The fast switching of the controller of (5) between the levels a and b determines an attraction of the state variable x_1 first to x_{1a} and then to x_{1b} , and so on. The fast switching between a and b , determines small variations of the state variables.

The dynamical state space trajectory remains around the equilibrium point, for each attractor starting from different initial conditions. With the anticontrol switching piecewise-constant controller of (5), the chaotic attractors are generated on the bold curve of Fig. 1. The study of the chaotic attractors shows an equidistant repartition in the state space. Figure 5 shows two transient state space trajectories until two independent chaotic attractors are reached.

The transitions $a \rightarrow b \rightarrow a \rightarrow b$ of the anticontrol switching piecewise-constant controller p of (5) determine a triangle characteristic of the transient state space trajectory. The times $(t_k)_{k \in \mathbb{N}}$ of the transitions $b \rightarrow a$ of p are symbolized by circles \bullet on the state space. At each time $(t_k)_{k \in \mathbb{N}}$, $g(t)$ is equal to $u(\mathbf{x}(t))$. Consequently, we can write:

$$g(t) = u(\mathbf{x}(t)). \quad (8)$$

According to (6), (8) becomes:

$$g(t) = \varepsilon \sin(\sigma x_1(t)). \quad (9)$$

For $t = t_0$, the solution of (9) is:

$$x_1(t_0) = \frac{1}{\sigma} \arcsin \frac{g(t_0)}{\varepsilon}. \quad (10)$$

The 2π periodicity of the sine function of $u(t)$ enables to find all the solutions $x_1(t_k)$ of (8):

$$\sigma x_1(t_k) \pm 2k\pi = \arcsin \frac{g(t_0)}{\varepsilon}, \quad k \in \mathbb{N}. \quad (11)$$

Then,

$$x_1(t_k) = \frac{1}{\sigma} \arcsin \frac{g(t_0)}{\varepsilon} \pm \frac{2k\pi}{\sigma}, \quad k \in \mathbb{N}. \quad (12)$$

We can also write:

$$x_1(t_k) - x_1(t_{k-1}) = \frac{2\pi}{\sigma}, \quad k \in \mathbb{N}^+. \quad (13)$$

We have demonstrated that the periodicity of the $x_1(t)$ function is $2\pi/\sigma$, i.e. the distance on the x_1 axis between two consecutive transitions $b \rightarrow a$ of p . Therefore, after many numerical simulations, we have deduced that the distance between two consecutive attractors on the x_1 axis coincides with the distance between two circles \bullet on the x_1 axis. Therefore, the attractors periodicity in the state space depends on the sine anticontrol feedback $u(\mathbf{x}(t))$ frequency given by the following relation:

$$d_{x_1} = \frac{2\pi}{\sigma}. \quad (14)$$

The d_{x_1} periodicity of attractors on the x_1 axis enables to find the maximal number of the attractors generated on the bold curve of Fig. 1, inside the x_1 state space domain $[x_{1a}; x_{1b}]$ of (4):

$$N_{\max} = \left\lceil \frac{x_{1b} - x_{1a}}{d_{x_1}} \right\rceil + 1. \quad (15)$$

N_{\max} of (15) gives the theoretical number of attractors that can be generated. The position of the first attractor generated inside the x_1 state space domain $[x_{1a}; x_{1b}]$ (near x_{1a}) cannot be controlled. On the other hand, the attractors which follow the first are equidistant, separated by a d_{x_1} distance. Two possible cases of repartition of chaotic attractors are given in Fig. 6. A difference of one attractor may sometimes occur between the theoretical and the simulated attractors number.

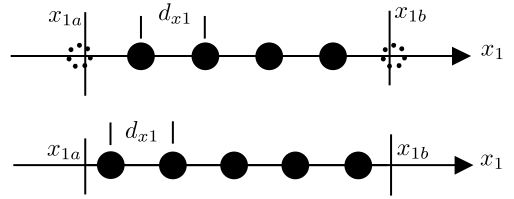


Fig. 6 Two possible attractors repartition inside the state space domain $[x_{1a}; x_{1b}]$ of (4)

The limit of the technique presented in this section is that the independent chaotic attractors cannot be generated on the entire state space for the nonlinear system of (1), using the anticontrol switching piecewise-constant controller of (5). Indeed, large values of x_1 change the dynamics of $u(\mathbf{x}(t))$, which gets closer to the fast dynamics of $g(t)$. The relation $\gamma > \sigma x_1$ must be verified to ensure that $g(t)$ has a faster dynamics than $u(\mathbf{x}(t))$. Therefore, the state space limit on the x_1 axis is γ/σ . Combining this limit with (2) enables the determination of the state space limits on all $x_2(t), \dots, x_N(t)$ axes.

In this section, we proposed a controller to generate several independent chaotic attractors in the state space. A control engineering application is to make nonlinear system converge to some attractors of interest, starting from different initial conditions, in order to reach different regimes of operation.

4 Lorenz system

In order to illustrate the proposed approach, the first example is based on the Lorenz system. This system has become a standard model for the study of chaos synchronization [1] and secure communications [4, 24]. The Lorenz system dynamics [14, 25] is described by the following parameterized equations in the dimensionless form:

$$\begin{cases} \dot{x}_1 = -\alpha(x_1 - x_2), \\ \dot{x}_2 = x_1 - x_2 - x_1 x_3 + p, \\ \dot{x}_3 = x_1 x_2 - \beta x_3, \end{cases} \quad (16)$$

with $\alpha = 10$, $\beta = \frac{8}{3}$. When $p = 0$, the Lorenz system (16) is not chaotic and, in fact, has the origin as a globally exponentially stable equilibrium point. Now, we use p as the control parameter. The parameterized

system Jacobian, evaluated at (x_1^*, x_2^*, x_3^*) , is given by

$$J_{x_1^*, x_2^*, x_3^*} = \begin{bmatrix} -\alpha & \alpha & 0 \\ 1 - x_3^* & -1 & -x_1^* \\ x_2^* & x_1^* & -\beta \end{bmatrix}. \quad (17)$$

The equilibria of the system (16) can be easily found by solving the three equations $\dot{x}_1 = \dot{x}_2 = \dot{x}_3 = 0$, which leads to

$$\begin{cases} -\alpha(x_1 - x_2) = 0, \\ x_1 - x_2 - x_1 x_3 + p = 0, \\ x_1 x_2 - \beta x_3 = 0. \end{cases} \quad (18)$$

Obviously, $S_0 = (0,0,0)$ is a trivial equilibrium. Linearizing the system (16) around the equilibrium S_0 provides three eigenvalues: $\lambda = 0, -\beta, -\alpha - 1$. The system has marginal stability. To find a nonzero equilibrium point, we may observe that the first equation in (18) yields immediately to $x_2 = x_1$, so that the third one gives $x_3 = \frac{x_1^2}{\beta}$ and the second one gives $p = \frac{x_1^3}{\beta}$. The system of (16) has one equilibrium point depending on the parameter p :

$$S = \left(\sqrt[3]{\beta p}, \sqrt[3]{\beta p}, \sqrt[3]{\frac{p^2}{\beta}} \right). \quad (19)$$

Linearizing the Lorenz system around the equilibrium point S yields the following Jacobian matrix and its characteristic equation:

$$J_S = \begin{bmatrix} -\alpha & \alpha & 0 \\ 1 - \sqrt[3]{\frac{p^2}{\beta}} & -1 & -\sqrt[3]{p\beta} \\ \sqrt[3]{p\beta} & \sqrt[3]{p\beta} & -\beta \end{bmatrix} \quad (20)$$

and

$$P(\lambda) = \lambda^3 + (\alpha + \beta + 1)\lambda^2 + \left[(\alpha + 1)\beta + (\alpha + \beta)\sqrt[3]{\frac{p^2}{\beta}} \right]\lambda + 3\alpha\beta\sqrt[3]{\frac{p^2}{\beta}}. \quad (21)$$

Let us apply now the Routh–Hurwitz criterion [9]: a necessary and sufficient condition for the stability of the equilibrium point S is that the real parts of the roots λ be negative, which can be confirmed if and only if the three following conditions hold:

$$\alpha + \beta + 1 > 0, \quad (22)$$

$$3\alpha\beta\sqrt[3]{\frac{p^2}{\beta}} > 0, \quad (23)$$

$$\begin{aligned} & (\alpha + \beta + 1) \left[(\alpha + 1)\beta + (\alpha + \beta)\sqrt[3]{\frac{p^2}{\beta}} \right] \\ & - 3\alpha\beta\sqrt[3]{\frac{p^2}{\beta}} > 0. \end{aligned} \quad (24)$$

The last Routh–Hurwitz condition leads to:

$$\begin{aligned} & (\alpha + \beta + 1)(\alpha + 1)\beta \\ & + [(\alpha - \beta)^2 + \alpha + \beta + \alpha\beta]\sqrt[3]{\frac{p^2}{\beta}} > 0. \end{aligned} \quad (25)$$

A static variation of p between a and b imposes the intervals to the equilibrium S on the x_1, x_2 and x_3 state space as following:

$$\text{on the } x_1 \text{ and } x_2 \text{ axes: } \left[\sqrt[3]{a\beta}, \sqrt[3]{b\beta} \right], \quad (26)$$

$$\text{on the } x_3 \text{ axis: } \left[\sqrt[3]{\frac{a^2}{\beta}}, \sqrt[3]{\frac{b^2}{\beta}} \right]. \quad (27)$$

We consider now a fast dynamics variation of p given by the anticontrol switching piecewise-constant controller p of (5). So, the independent chaotic attractors are generated inside the state space of (26) and (27). Taking into account the distance between two consecutive attractors on the x_1 axis given by (14), the maximum number of independent chaotic attractors of (15) generated on the interval of (26) is described by:

$$N_{\max} = \left\lceil \frac{\sigma\sqrt[3]{\beta}}{2\pi} (\sqrt[3]{b} - \sqrt[3]{a}) \right\rceil + 1. \quad (28)$$

In our simulations, $\gamma = 1000$, $\sigma = 100$ and $\varepsilon = 5$. With this values, (22), (23), (25) hold, therefore the equilibrium point S of the system of (16) is always stable.

We list in Table 1 the equilibria intervals on each axis x_1, x_2 and x_3 (derived from (26) and (27)) for three different values of a and b . This table includes the maximum number of chaotic attractors of (28), which could be generated from different initial conditions.

Let us see now if the results of the numerical simulations are in concordance with those given in Table 1 by the mathematical formula (26)–(28). Figure 7 shows the independent chaotic attractors of the Lorenz

Table 1 Lorenz system

a	b	x_1, x_2 of (26)	x_3 of (27)	N_{\max} of (28)
0	0.5	[0, 1.1]	[0, 0.45]	18
1	2	[1.3867, 1.747]	[0.721, 1.145]	6
-1.5	-0.5	[-1.587, -1.1]	[0.454, 0.945]	8

system (16) and their projections onto x_1 - x_3 plane respectively. The attractors, generated from different initial conditions, are situated in the plane $x_1 = x_2$, and on the parabola $x_3 = 3x_1^2/8$ represented in Fig. 7 with the fine curve. For the three intervals of p , the attractors projections onto x_1 - x_3 plane shows that all the attractors are situated inside the state space given by Table 1 (third and fourth columns). On the other hand, there is a difference of one attractors between the numerical simulation of the independent chaotic attractors number generated on the interval of (26) and the maximum number of attractors given by the mathematical formula of (28). These three cases correspond to the first case of attractors repartition inside the state space domain $[x_{1a}; x_{1b}]$ of (4) is available, as in Fig. 6.

Figure 8 presents the projections of one attractor onto x_1 - x_2 plane. This attractor reaches the regime of operation $x_1 = 0.6$, $x_2 = 0.6$ and $x_3 = 0.135$.

The positive largest Lyapunov exponent has become the standard characteristics of a chaotic system. At the end of the present section, we introduce the Lyapunov exponent as a simple measure of sensitive dependence on initial conditions, distinguishing a chaotic from a nonchaotic trajectory by its positive value.

For a linear increasing variation of ε parameter, the Lyapunov exponent has positive values as in Fig. 9, decreasing to negative values. The Lyapunov exponent of the Lorenz system (16) is calculated for distinct initial conditions (almost identical) near an equilibrium point (i.e. near the basin of attraction). With almost identical initial conditions, but far away of the equilibrium points (outside of the basin of attraction), the Lorenz system (16) could reach different regimes of operation (two different attractors), as in Fig. 10. This choice of initial conditions is a source of errors in the calculation of the Lyapunov exponent.

In this section, we show that the switching piecewise-constant controller of (5)–(7) can drive the Lorenz system from nonchaotic (with zero equilibrium point) to chaotic (with several equilibria points) behaviors.

5 Van der Pol system

In this section, we generate independent chaotic attractors from the Van der Pol system [26, 27], which can be written by the following equations:

$$\begin{cases} \dot{x}_1 = x_2, \\ \dot{x}_2 = -x_1 - 3 \cdot (x_1^2 - 1)x_2 + p. \end{cases} \quad (29)$$

Without switching piecewise-constant controller (i.e., when $p = 0$), the Van der Pol system (29) has a one period limit cycle, as shown in Fig. 11.

The corresponding Jacobian matrix evaluated at (x_1^*, x_2^*) is

$$J_{x_1^*, x_2^*} = \begin{bmatrix} 0 & 1 \\ -1 - 6x_1^*x_2^* & 3(1 - x_1^{*2}) \end{bmatrix}. \quad (30)$$

The equilibria of the system (29) are found by solving the equations $\dot{x}_1 = \dot{x}_2 = 0$, which leads to the following relations:

$$x_2 = 0, \quad x_1 = p. \quad (31)$$

The Van der Pol system of (29) has one equilibrium point:

$$S = (p, 0). \quad (32)$$

To study the stability of S , we compute the Jacobian J_S evaluated for this equilibrium, as follows:

$$J_S = \begin{bmatrix} 0 & 1 \\ -1 & 3(1 - p^2) \end{bmatrix}. \quad (33)$$

Linearizing the system (29) around S provides the following characteristic equation:

$$P(\lambda) = \lambda^2 - 3(1 - p^2)\lambda + 1. \quad (34)$$

The Routh–Hurwitz conditions lead to the relation:

$$p^2 - 1 > 0, \quad \text{so } p \in (-\infty, -1) \cup (1, +\infty). \quad (35)$$

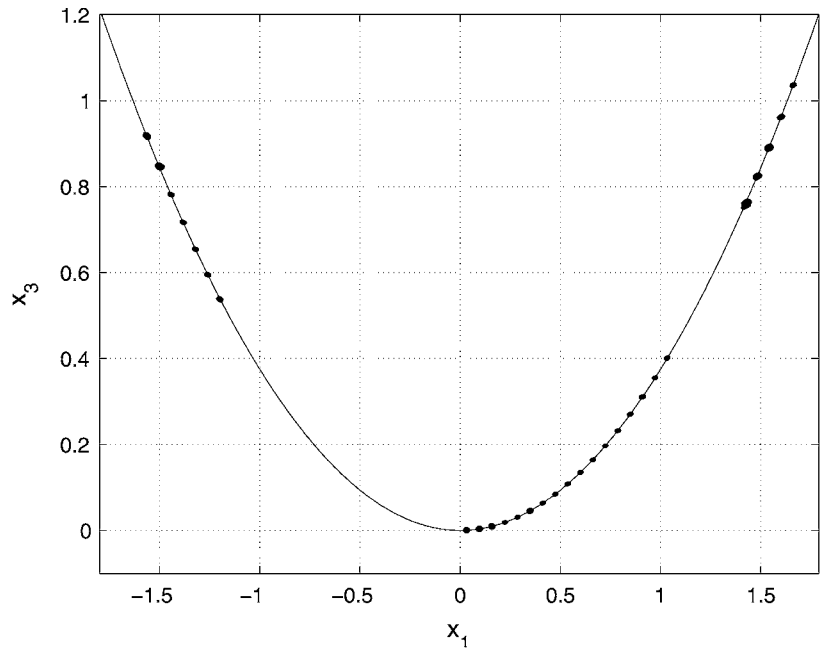
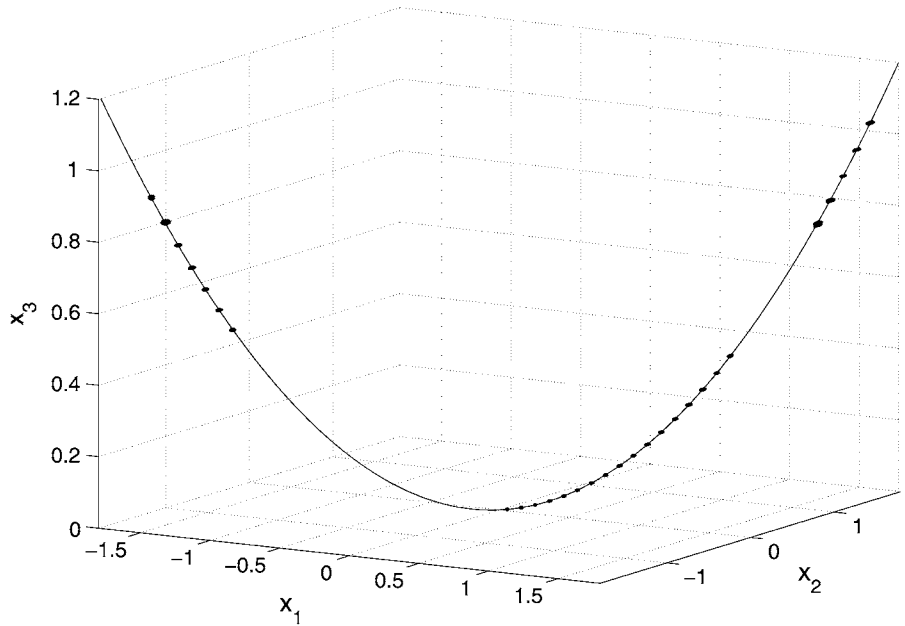
Therefore, the stability of the equilibrium point S depends on the p values. The annulation of \dot{x}_2 determines a direct relationship between p and x_1 :

$$p = x_1. \quad (36)$$

As discussed previously, (36) and (31) enable the calculation of equilibria intervals for a variation of p between the limits a and b :

$$\text{on the } x_1 \text{ axis: } [a, b]. \quad (37)$$

Fig. 7 The independent chaotic attractors of the Lorenz system (16) and their projections onto x_1-x_3 plane



The independent chaotic attractors are generated inside the state space of (37) around $x_2 = 0$.

Dividing the interval of (37) with the distance between two consecutive attractors, we determine the maximal number of attractors which can be generated in the state space:

$$N_{\max} = \left\lceil \frac{x_{1b} - x_{1a}}{d_{x1}} \right\rceil + 1 = \left\lceil \frac{\sigma}{2\pi} (b - a) \right\rceil + 1. \quad (38)$$

We consider the anticontrol switching piecewise constant controller p given by (5). We take the same values as for the Lorenz system: $\gamma = 1000$, $\sigma = 100$ and $\varepsilon = 5$.

Fig. 8 A chaotic attractor of the Lorenz system (16); the attractor projection onto x_1-x_2 plane

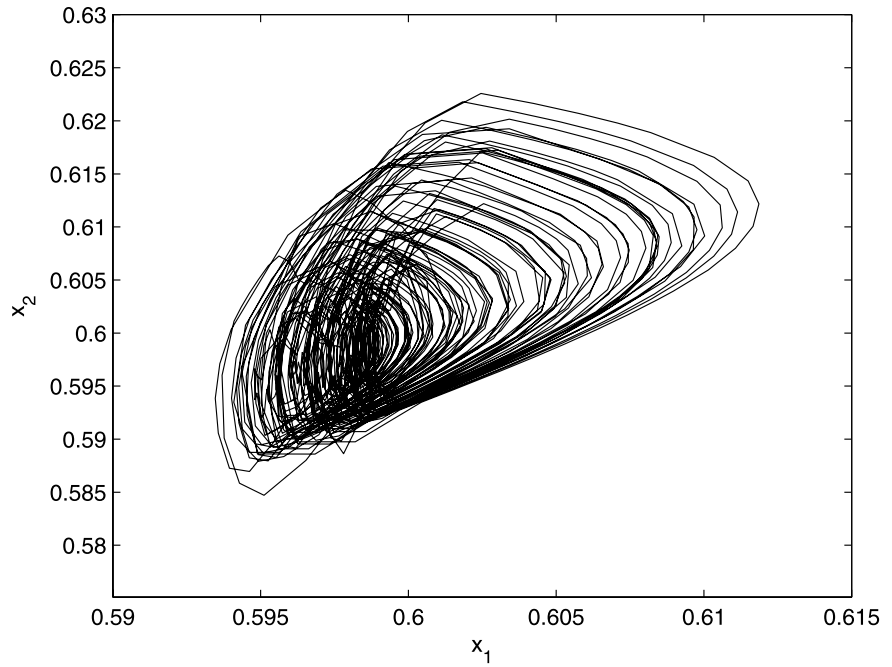


Fig. 9 The largest Lyapunov exponents of the Lorenz system (16)

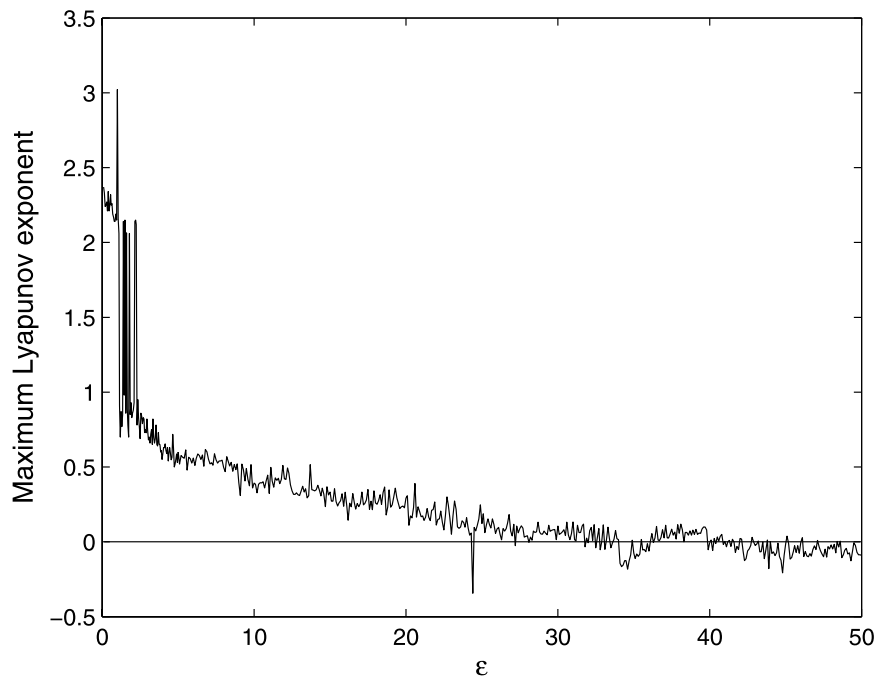


Table 2 contains the maximal attractors number AN_{\max} of (38) which can be generated inside the state domain x_1 of (37) (around $x_2 = 0$) for three different controllers p .

The numerical simulations of the Van der Pol system (29) present independent chaotic attractors, as shown in Fig. 12. The attractors, generated from different initial conditions, are situated on the line

Fig. 10 The time waveform of the x_1 state variable of the Lorenz system (16) starting from distinct initial conditions (almost identical) far away of the equilibrium points

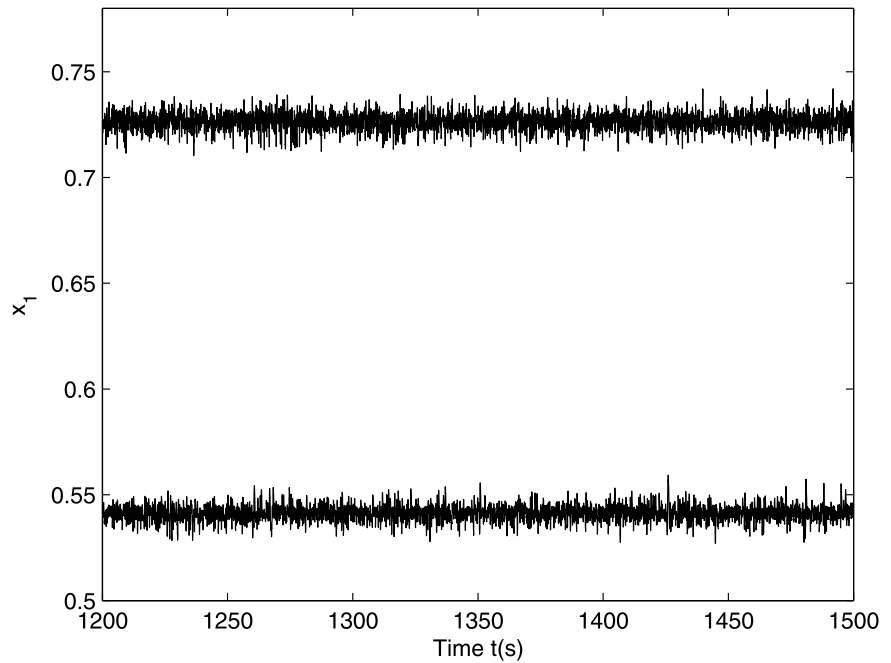
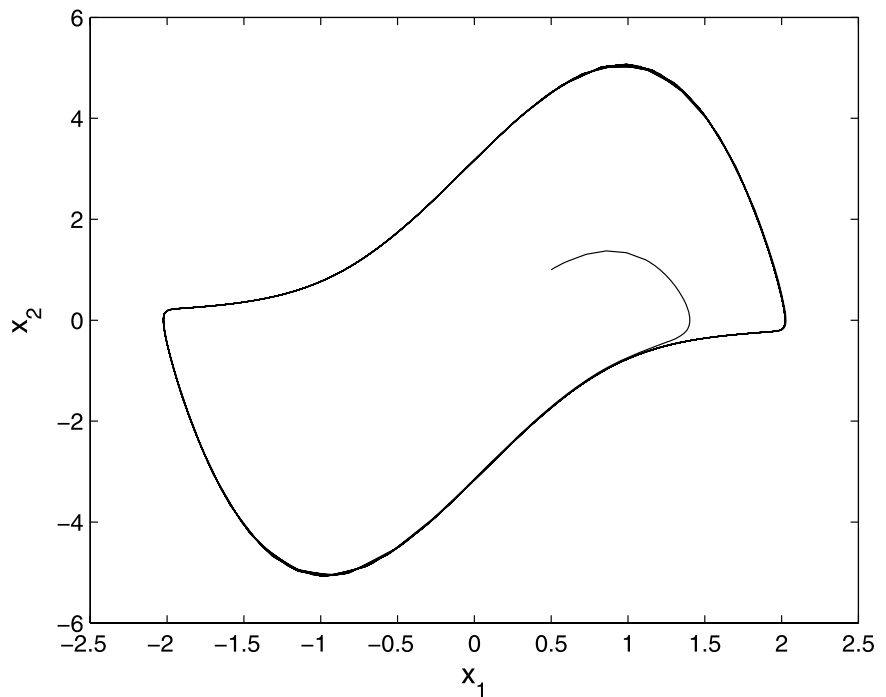


Fig. 11 One period limit cycle of the Van der Pol system (29) with $p = 0$



$x_2 = 0$ represented in the Fig. 12 with the fine curve.

For the three intervals of p , the projections of the attractors onto x_1-x_2 plane show that all at-

tractors are situated inside the state space given by Table 2 (third column). For each particular value of the anticontrol switching piecewise-constant controller p , Fig. 12 presents sixteen attractors obtained

Fig. 12 Independent chaotic attractors of the Van der Pol system (29)

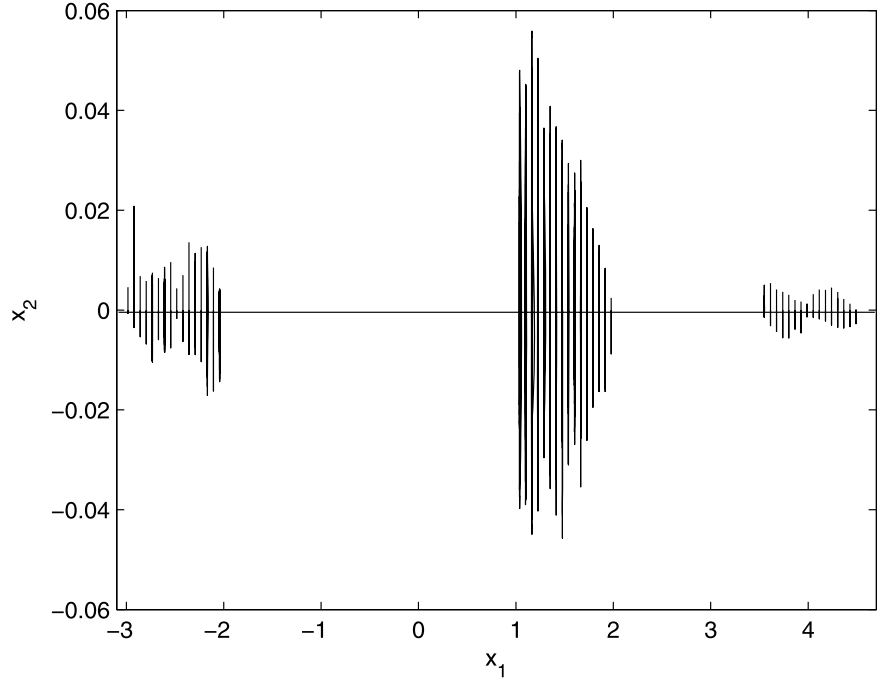


Table 2 Van der Pol system

a	b	x_1 of (37)	N_{\max} of (38)
1	2	[1; 2]	16
3.5	4.5	[3.5; 4.5]	16
-3	-2	[-3; -2]	16

by simulation. The mathematical formula of (38) gives the same number of attractors. The second case of attractors repartition inside the state space domain $[x_{1a}; x_{1b}]$ of (4) is therefore fulfilled, as in Fig. 6.

Figure 13 presents the projections of one attractor onto the x_1 - x_2 plane. Considering ε as parameter, the maximum Lyapunov exponent of the Van der Pol system (29) is shown in Fig. 14. Its positive value demonstrates the chaotical behavior of the Van der Pol system (29).

According to the above analysis, we use the switching piecewise-constant controller of (5)–(7) to make the Van der Pol system chaotic (with several equilibria points) from a one period limit cycle.

6 Jerk system

Let us take another example, a special class of three-dimensional dynamical systems, the so-called Jerk system [11]. The general Jerk system is described by $\ddot{x} + A\dot{x} + Bx = g(x)$, where A, B are real parameters and $g(x)$ a nonlinear function; the first derivative \dot{x} is called velocity, the second \ddot{x} is called acceleration, and the third \dddot{x} is called Jerk. Linz [28] and Sprott [29] investigated the dynamical behavior of this system with the nonlinear function $g(x) = 1 - |x|$. The inclusion of the anticontrol switching piecewise-constant controller p in the Jerk system is described by:

$$\begin{cases} \dot{x}_1 = x_2 + p, \\ \dot{x}_2 = x_3, \\ \dot{x}_3 = -Ax_3 - Bx_2 - |x_1| + 1. \end{cases} \quad (39)$$

When $p = 0$, the Jerk system (39) is not chaotic and it has $(1, 0, 0)$ as the stable equilibrium point.

Using p as the control parameter, the equilibria of the system (39) can be found by solving $\dot{x}_1 = \dot{x}_2 = \dot{x}_3 = 0$, which leads to: $x_2 = -p$, $x_3 = 0$, and $|x_1| = 1 - Bx_2$. We find two equilibria S_+ and S_- , symmetrically placed with respect to the x_1 -axis:

Fig. 13 Independent chaotic attractors of the Van der Pol system (29)

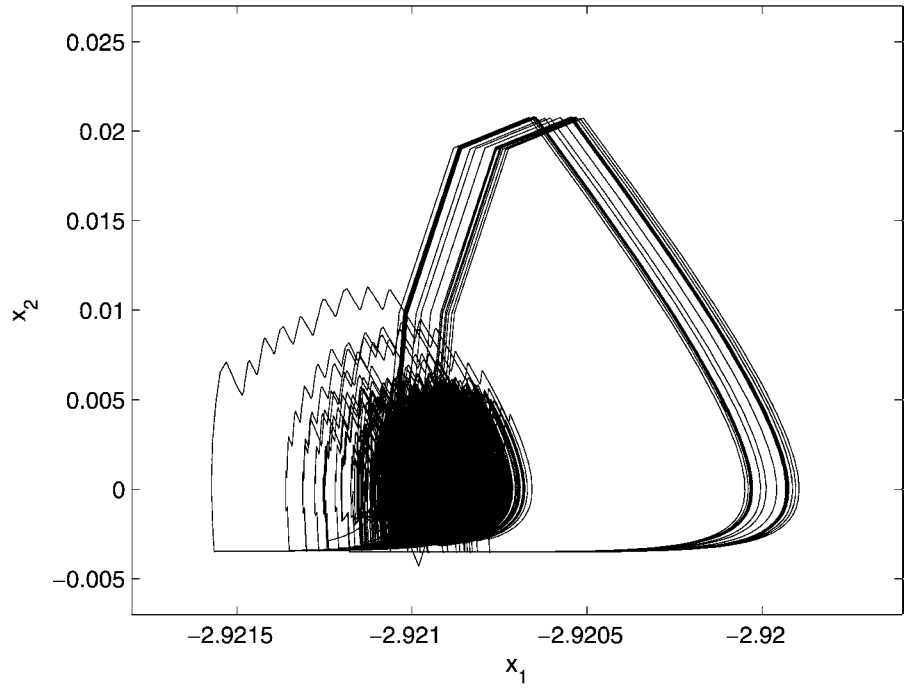
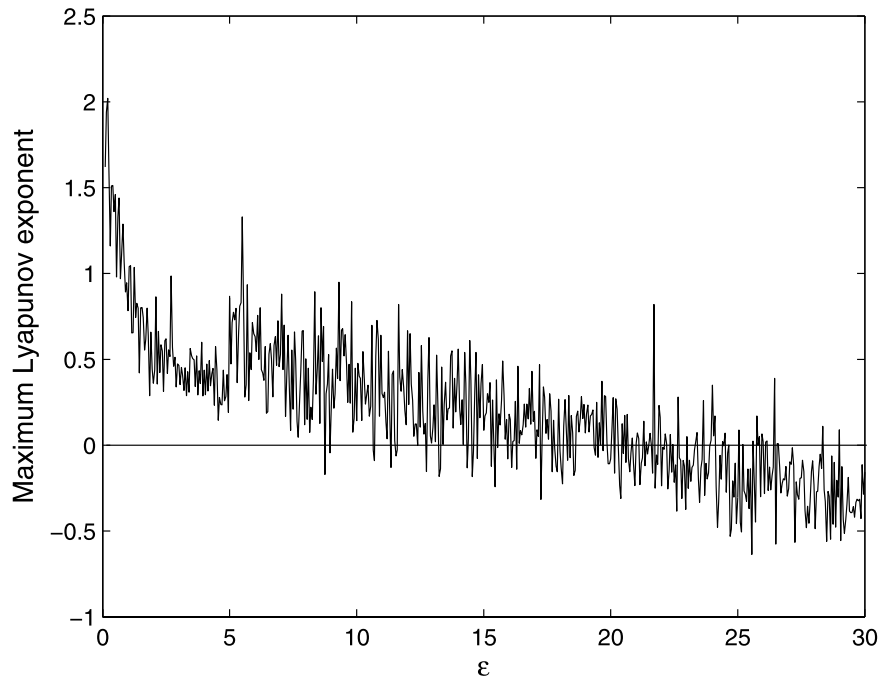


Fig. 14 The maximum Lyapunov exponents of the Van der Pol system (29)



$$S_+ = (Bp + 1, -p, 0)$$

and

$$S_- = (-Bp - 1, -p, 0).$$

(40)

Considering a Jacobian matrix for one of these equilibria and calculating its characteristic equation, we can investigate the stability of this equilibrium based on the Routh–Hurwitz conditions on the Jerk system (39)

characteristic equation. Therefore:

$$P(\lambda) = \lambda^3 + A\lambda^2 + B\lambda + 1. \quad (41)$$

A necessary and sufficient condition for the stability of the equilibrium points S_+ and S_- is given by the condition: $A > 0$ and $AB - 1 > 0$.

Table 3 Jerk system

c	d	x_2 of (43)	p of (44), (45)	N_{\max} of (46)
-3	-2.25	[-2, -1.25]	[1.25, 2]	12
1.25	2	[-1, -0.25]	[0.25, 1]	12
-0.8	0	[0.2, 1]	[-1, -0.2]	13

Fig. 15 Independent chaotic attractors of the Jerk system of (39) and their projections onto the x_1 - x_2 plane

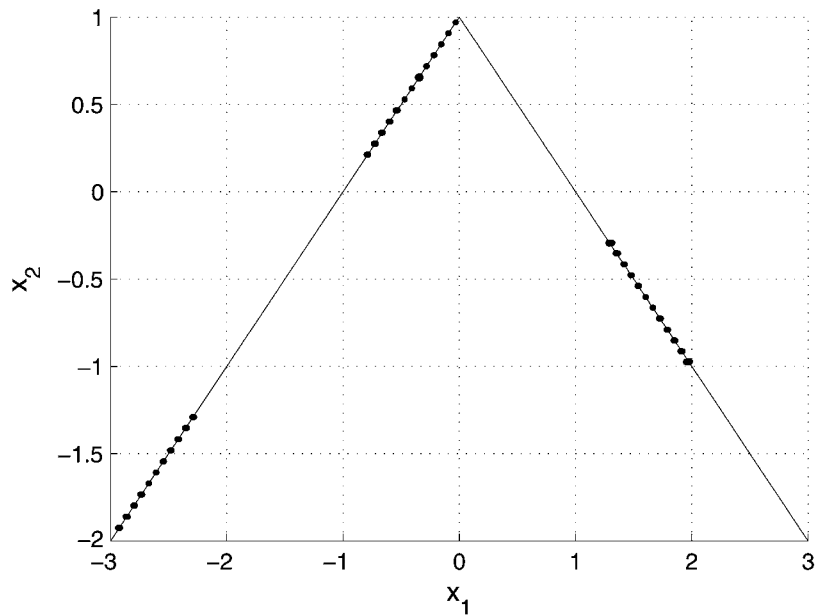
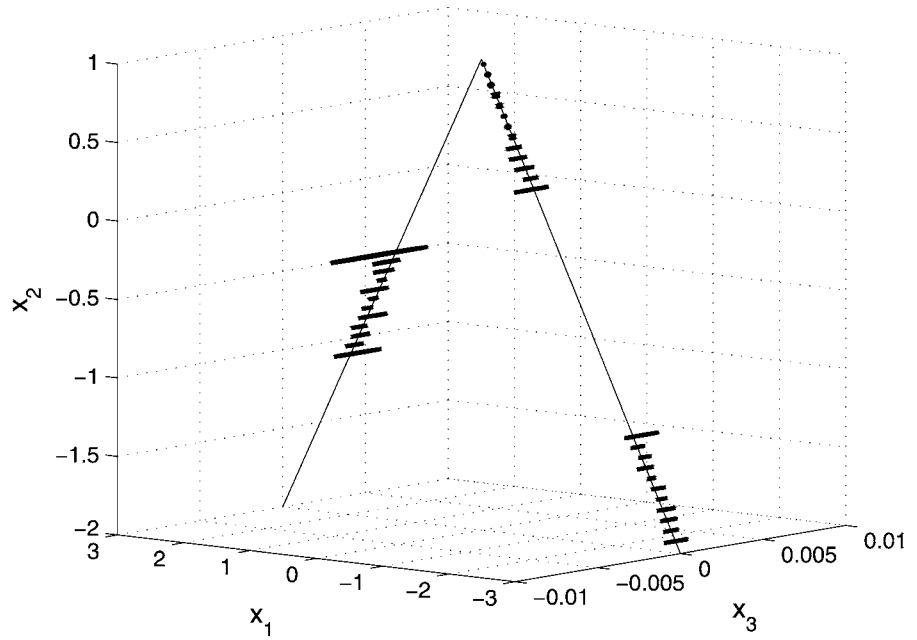
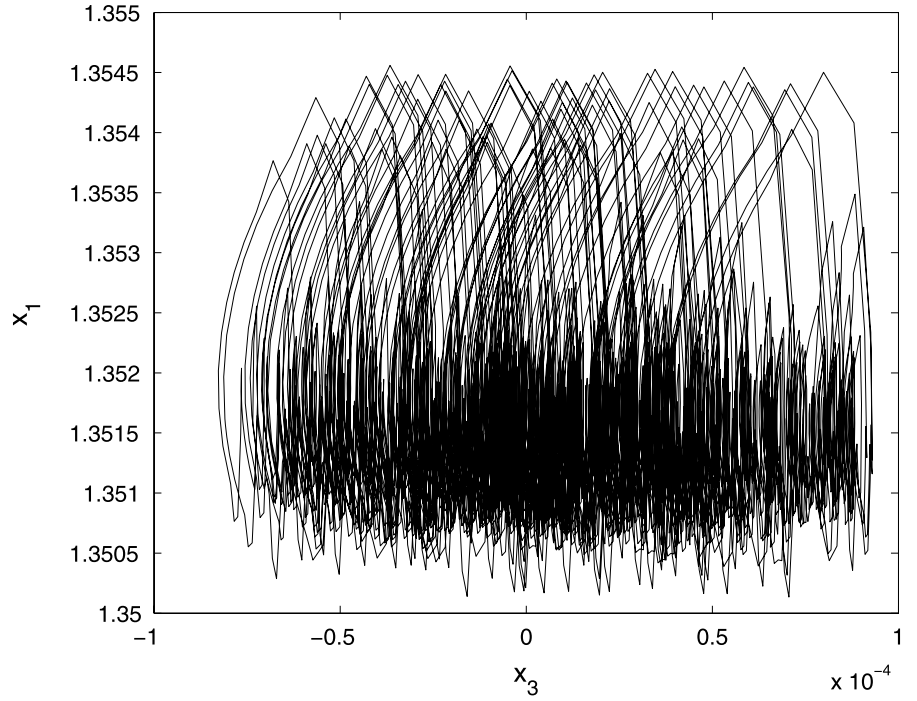


Fig. 16 Projection of a chaotic attractor of the Jerk system of (39)



This time, we want to have chaotic attractors on the state space between the limits c and d for an x_1 axis projection:

$$\text{on the } x_1 \text{ axis: } [c; d]. \quad (42)$$

The state space domain for an x_2 axis projection is:

$$\text{on the } x_2 \text{ axis: } \begin{cases} \left[\frac{1}{B}(1-d), \frac{1}{B}(1-c) \right], & \text{if } c \geq 0 \\ \left[\frac{1}{B}(1+c), \frac{1}{B}(1+d) \right], & \text{if } c < 0. \end{cases} \quad (43)$$

Substituting (43) into $x_2 = -p$, the anticontrol switching piecewise-constant controller p has the following form:

$$\text{if } c \geq 0, \quad p = \begin{cases} \frac{1}{B}(c-1), & g(t) \geq u(\mathbf{x}(t)) \\ \frac{1}{B}(d-1), & g(t) < u(\mathbf{x}(t)), \end{cases} \quad (44)$$

and

$$\text{if } c < 0, \quad p = \begin{cases} \frac{1}{B}(-1-d), & g(t) \geq u(\mathbf{x}(t)) \\ \frac{1}{B}(-1-c), & g(t) < u(\mathbf{x}(t)). \end{cases} \quad (45)$$

The number of attractors is:

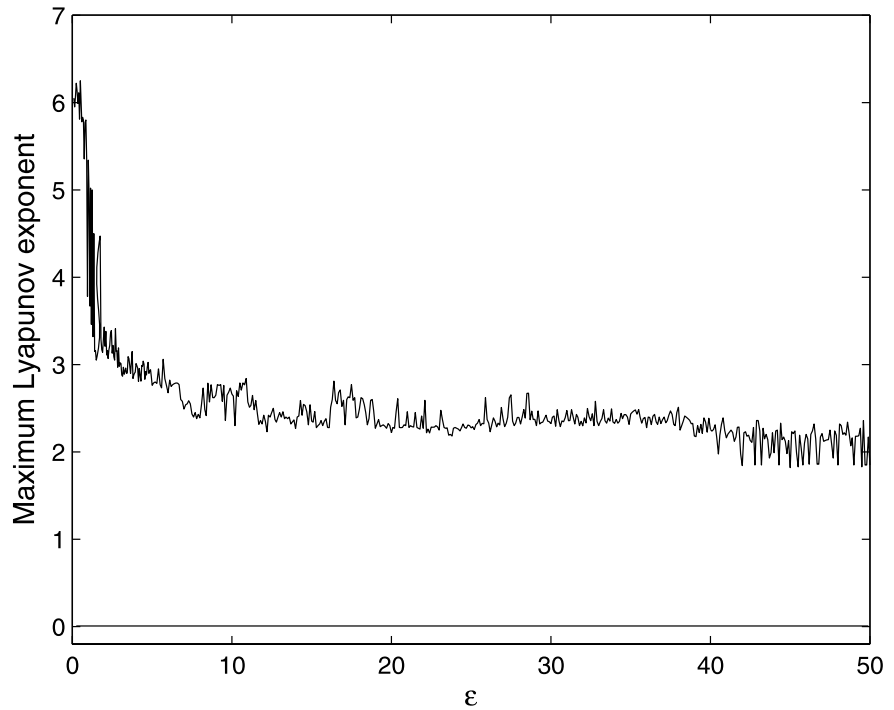
$$N_{\max} = \left\lceil \frac{\sigma}{2\pi} (d-c) \right\rceil + 1. \quad (46)$$

For the numerical simulation, let us assume, as in [29], that $A = 2.017$ and $B = 1$. For these values, the equilibrium points S_+ and S_- are stable. Let us take the same expressions for the functions $g(t)$ and $u(\mathbf{x}(t))$ as in the Lorenz and Van der Pol systems.

Table 3 presents limits imposed to the state space domain for an x_1 axis projection (c and d), the state space domain for an x_2 axis projection calculated with (43), the switch levels of the anticontrol switching piecewise-constant controller p of (44) and (45) and the maximum number of chaotic attractors (46) which can be generated.

For three values of the anticontrol switching piecewise-constant controller p (fourth column of Table 3), Fig. 15 presents three groups of independent chaotic attractors and their projections onto the x_1 - x_2 plane, respectively. The first case of attractors repartition inside the state space domain $[x_{1a}; x_{1b}] = [-3; -2.25]$ of (4) is available. This is why there is a difference of one attractor between the numerical simulation of the independent chaotic attractors number generated and the maximum of the attractors num-

Fig. 17 The maximum Lyapunov exponents of the Jerk system (39)



ber given by (46). For the two other state space domains $[x_{1a}; x_{1b}] = [-0.8; 0]$ and $[x_{1a}; x_{1b}] = [1.25; 2]$, the theoretical and simulated attractors number coincide.

The projection of a chaotic attractor of the Jerk system of (39) is shown on Fig. 16, together with the largest Lyapunov exponent presented in Fig. 17.

As for the Lorenz system, we show that the switching piecewise-constant controller of (5)–(7) can drive the Jerk system from a nonchaotic (with $(1, 0, 0)$ equilibrium point) to a chaotic (with several equilibria points) behavior.

7 Conclusion

The present paper introduces a new technique to generate independent chaotic attractors using a switching piecewise-constant controller in continuous-time nonchaotic systems (with an equilibrium point or a limit cycle). We demonstrate here that the equidistant repartition of these attractors is in a precise zone (a controllable state space area) of the precise curve, which depends of the system parameters. We determine the state space domains where the attractors are generated

from different initial conditions. A mathematical formula giving the maximal attractors number in function of the controller piecewise-constant values is then deduced. A control engineering application can be to make a nonlinear system converge to some attractors of interest, starting from different initial conditions, in order to reach different regimes of operation.

References

1. Fujisakaa, H., Yamadab, T., Kinoshitaa, G., Konoa, T.: Chaotic phase synchronization and phase diffusion. *Physica D* **205**, 41–47 (2006)
2. Mahmoud, G.M., Aly, S.A., Al-Kashif, M.A.: Dynamical properties and chaos synchronization of a new chaotic complex nonlinear system. *Nonlinear Dyn.* **51**, 171–181 (2006)
3. Warminski, J., Litak, G., Szabelski, K.: Synchronisation and chaos in a parametrically and self-excited system with two degrees of freedom. *Nonlinear Dyn.* **22**, 135–153 (2000)
4. Alvarez, G., Montoya, F., Romera, M., Pastor, G.: Breaking two secure communication systems based on chaotic masking. *IEEE Trans. Circuits Syst. II* **51**, 505–506 (2004)
5. Lukac, R., Plataniotis, K.: Bit-level based secret sharing for image encryption. *Pattern Recognit.* **38**, 767–772 (2005)
6. Deane, J., Ashwin, P., Hamill, D., Jefferies, D.: Calculation of the periodic spectral components in a chaotic DC–DC converter. *IEEE Trans. Circuits Syst. I* **46**, 1313–1319 (1999)

7. Lü, J., Yu, X., Chen, G.: Generating chaotic attractors with multiple merged basins of attraction: A switching piecewise-linear control approach. *IEEE Trans. Circuits Syst. I* **50**, 198–207 (2003)
8. Lü, J., Yu, X., Zhou, T., Chen, G., Yang, X.: Generating chaos with a switching piecewise-linear controller. *Chaos* **12**, 344–349 (2002)
9. Aziz-Alaoui, M., Chen, G.: Asymptotic analysis of a new piecewise-linear chaotic system. *Int. J. Bifurc. Chaos* **12**, 147–157 (2002)
10. Ueta, T., Chen, G.: Bifurcation analysis of Chen's equation. *Int. J. Bifurc. Chaos* **10**, 1917–1931 (2000)
11. Yu, S., Lü, J., Leung, H., Chen, G.: Design and implementation of N-scroll chaotic attractors from a general Jerk circuit. *IEEE Trans. Circuits Syst. I* **52**, 1459–1476 (2005)
12. Tang, W., Zhong, G., Chen, G., Man, K.: Generation of N-scroll attractors via sine function. *IEEE Trans. Circuits Syst. I* **48**, 1369–1372 (2001)
13. Li, Z., Park, J., Chen, G., Young, H., Choi, Y.: Generating chaos via feedback control from a stable TS fuzzy system through a sinusoidal nonlinearity. *Int. J. Bifurc. Chaos* **12**, 2283–2291 (2002)
14. Wang, X., Chen, G., Yu, X.: Anticontrol of chaos in continuous-time systems via time-delay feedback. *Chaos* **10**, 771–779 (2000)
15. Peng, M.S.: Bifurcation and chaotic behavior in the Euler method for a Kaplan–Yorke prototype delay model. *Chaos Solitons Fractals* **20**, 489–496 (2004)
16. Peng, M.S., Ucar, A.: The use of the Euler method in identification of multiple bifurcations and chaotic behavior in numerical approximations of delay differential equations. *Chaos Solitons Fractals* **21**, 883–891 (2004)
17. Peng, M.: Symmetry breaking, bifurcations, periodicity and chaos in the Euler method for a class of delay differential equations. *Chaos Solitons Fractals* **24**, 1287–1297 (2005)
18. Kennedy, M.: Three steps to chaos—Part I: Evolution. *IEEE Trans. Circuits Syst. I* **40**, 640–656 (1993)
19. Endersen, L., Skarland, N.: Limit cycle oscillations in pacemaker cells. *IEEE Trans. Biomed. Eng.* **47**, 1–5 (2000)
20. Morel, C., Bourcier, M., Chapeau-Blondeau, F.: Improvement of power supply electromagnetic compatibility by extension of chaos anticontrol. *J. Circuits Systems Comput.* **14**, 757–770 (2005)
21. Morel, C., Vlad, R., Morel, J.-Y.: Anticontrol of chaos reduces spectral emissions. *J. Comput. Nonlinear Dyn.* **3**, 041009-1–041009-6 (2008)
22. Fouladgar, J., Chauveau, E.: The influence of the harmonics on the temperature of electrical machines. *IEEE Trans. Magn.* **41**, 1644–1647 (2005)
23. Morel, C., Bourcier, M., Chapeau-Blondeau, F.: Generating independent chaotic attractors by chaos anticontrol in nonlinear circuits. *Chaos Solitons Fractals* **26**, 541–549 (2005)
24. Li, C., Liao, X., Wong, K.: Chaotic lag synchronization of coupled time-delayed systems and its applications in secure communication. *Physica D* **194**, 187–202 (2004)
25. Mello, L., Messias, M., Braga, D.: Bifurcation analysis of a new Lorenz-like chaotic system. *Chaos Solitons Fractals* **37**, 1244–1255 (2008)
26. Mahmoud, G.M., Farghaly, A.A.M.: Chaos control of chaotic limit cycles of real and complex Van der Pol oscillators. *Chaos Solitons Fractals* **21**, 915–924 (2004)
27. Hirano, N., Rybicki, S.: Existence of limit cycles for coupled Van der Pol equations. *J. Differ. Equ.* **195**, 194–209 (2003)
28. Linz, S., Sprott, J., Leung, H., Chen, G.: Elementary chaotic flow. *Phys. Lett. A* **259**, 240–245 (1999)
29. Sprott, J.: A new class of chaotic circuit. *Phys. Lett. A* **266**, 19–23 (2000)